ARTIFICIAL NEURAL NETWORK MODEL FOR INTEGRATING ELECTRICAL RESISTIVITY AND PENETRATION RESISTANCE OF ALLUVIAL SOILS USING TENSOR FLOW-KERAS-DRIVEN BACKPROPAGATION FEEDFORWARD ANALYSIS & HYPERPARAMETER TUNING

M. Rafique[1] M. Arqam[2,] and H. Ajmal[3]

[2] Institute of Geology, University of the Punjab, P.O. Box No. 54590. Lahore, Pakistan
[2,3]Department of Civil Engineering, University of Engineering & Technology, 39161, Lahore, Pakistan
Corresponding Author: [1]Muhammad Arqam 2020civ15@student.uet.edu.pk

ABSTRACT: This study presents an integrated approach combining Electrical Resistivity Survey (ERS) and Standard Penetration Test (SPT-N) data to improve subsurface characterization in alluvial soils, overcoming limitations of conventional drilling methods including logistical difficulties in mobilizing rotary drilling rigs measurement errors, high costs, and terrain constraints in difficult low-accessibility areas. A novel multivariate Artificial Neural Network (ANN) framework was developed using TensorFlow-Kera's, implementing feedforward architecture with backpropagation learning. The model incorporates an innovative hyperparameter tuning protocol that systematically evaluates network depth (1-5 hidden layers) and complexity (2-10 neurons/hidden layer), identifying a 4-layer configuration provide optimal predictive accuracy (adjusted R^2 = 0.99, RMSE = 6.36, MAPE = 1.1%, MSLE =0.01) with effectively balancing between both underfitting and overfitting tendencies. The finalized model transforms ERS and SPT-N inputs into predictive multivariate regression equations for key geotechnical parameters estimations & foundation design analyses by applying backpropagations feedforward analysis on well trained & tested modular weight-bias matrixes of each hidden layer. This methodology advances Sustainable Development Goal 9 (SDG 9) by enabling efficient, non-invasive subsurface investigations in challenging environments (floodplains, remote areas). Specifically, it addresses Target 9.1 (resilient infrastructure development) and Target 9.4 (sustainable industrialization) through its reduced reliance on conventional drilling, demonstrating how machine learning can enhance geotechnical practice while supporting sustainable infrastructure planning.

Keywords: Artificial Neural Networks (ANN), Electrical Resistivity, Standard Penetration Test (SPT-N), Hyperparameter Tuning, TensorFlow-Keras Backpropagation, Mean Absolute Percentage Error (MAPE).

INTRODUCTION

Recent advancements in subsurface characterization have increasingly focused on the integration of machine learning (ML) with traditional geophysical and geotechnical investigation techniques. This convergence is transforming how engineers interpret subsurface data and predict soil behavior, especially in data-scarce or difficult-to-access environments.

A comprehensive review presented by the authors of Machine Learning-Aided Characterization Using Geophysical Data Modalities (2022) outlines how ML can collaborate with physics-based models to improve resolution, reliability, and interpretation of subsurface features.Lozić and Mirčeta (2024) demonstrated the effectiveness of ML by jointly analyzing geophysical and borehole data in karst environments.

Their work, centered on the Gusić Polje 2 Compensation Basin for the Senj 2 Hydroelectric Power Plant, developed a 3D spatial model that predicted ground settlement while mapping uncertainty. Similarly, Li (2020) addressed data scarcity issues by integrating seismic survey results, well logs, and core samples using ML algorithms.

This integration enhanced subsurface interpretation through synthetic log generation, fracture detection, and reinforcement learning for automatic history matching.

In mineral exploration, Balaguera et al. (2024) employed ML to predict petrophysical properties and classify lithofacies at the Riotinto mine, while Horrocks (2019) successfully developed ML workflows that synthesized geological logs, multi-element geochemical assays, and 3D geophysical inversion models at the Kevitsa Ni-Cu-PGE deposit in Finland. These studies highlight the growing reliability of ML in diverse geological conditions.

In conventional geotechnical practice, the Standard Penetration Test (SPT) remains a widely used tool for evaluating soil resistance. It informs essential parameters like internal friction angle, unit weight, cohesion, and modulus of elasticity (Cosenza et al., 2006; Jay, Ameratunga, Sivakugan, Das, 2016). However, SPT is often considered time-consuming and expensive (Schmertmann, 2008; Adewoyin et al., 2017). Especially in remote or logistically challenging areas, traditional SPT campaigns are frequently limited due to equipment constraints and cost (Gordon and Fletcher, 1965; Yusuf and Kurniawan, 2024).

In response, geophysical techniques have gained traction as rapid, cost-effective, and non-invasive alternatives. Among these, Electrical Resistivity Surveys (ERS) are increasingly adopted for engineering site characterization, as noted by Samouëlian et al. (2005), Cosenza et al. (2006), Pozdnyakov et al. (2006), and Siddiqui and Osman (2013). The ERS method, especially Vertical Electrical Sounding (VES), offers a simple and economical means of gathering subsurface data. Baharom, Azahar, Syed, Irfan, and Siddiqui (2012) identified ERS as a viable complement or substitute to SPT, particularly in terrains where drilling is challenging.

Establishing empirical correlations between geophysical properties (e.g., electrical resistivity) and geotechnical parameters (e.g., SPT-N values) has become essential. Islam et al. (2020) showed that reliable correlations between resistivity and SPT can improve geotechnical evaluations and soil classification. Numerous studies have attempted to establish such relationships, exploring how resistivity varies with index properties like compaction, texture, and moisture content (Mariusz et al., 2020; Wasayo and Sahito, 2023; Juliana et al., 2021). The underlying principle is that both electrical resistivity and SPT-N values exhibit depth-dependent variation due to changes in soil density and shear strength.

F.I. Siddiqui and S.B.A.B.S. Osman (2013), along with S.N. Mohd Akip Tan et al. (2018), explored correlations between SPT-N and resistivity across different soil profiles. Additional correlations with soil plasticity, cohesion, and friction angle have also been examined (Sinta et al., 2018; Kibria and Hossain, 2012).

Beyond SPT correlations, electrical resistivity has been linked to a range of geotechnical and hydraulic parameters, including water content, salinity, thermal resistivity, cation exchange capacity (CEC), and hydraulic conductivity (Abu-Hassanein et al., 1996; Erzin et al., 2010; Kalinski and Kelly, 1993, 1994; McCarter, 1984; Pozdnyakova et al., 2001; Schwartz et al., 2008; Son et al., 2009).

Notably, Cosenza et al. (2006) conducted a 2D resistivity survey using a Wenner array, while Sudha et al. (2009) demonstrated site-specific correlations between 2D tomography results and SPT data. However, Braga et al. (1999) observed a weak relationship between SPT and resistivity in sandy-clay formations, indicating the need for site-specific calibration. Liu et al. (2008) and Oh and Sun (2008) reported strong correlations between resistivity and both SPT and compressive strength in soil-cement mixtures and earth dams, respectively.

Despite the success of these studies, many relied on costly hardware, advanced electrode switching devices, and proprietary data inversion software. Their complex nature and demand for skilled personnel increase implementation costs (Cosenza et al., 2006; Liu et al., 2008; Oh and Sun, 2008; Sudha et al., 2009).

Crucially, none of these studies examined the correlation between SPT and electrical resistivity obtained via the simpler and more affordable Vertical Electrical Sounding (VES) method (Fahad Irfan Siddiqui and Baharom Azahar Syed, 2012). This presents an opportunity for developing data-driven machine learning models that exploit low-cost VES data to estimate geotechnical properties, such as SPT-N values, especially in areas where traditional testing is infeasible.

By combining ERS data with ML algorithms and SPT-based field records, robust correlation models can be developed to aid in soil classification, compaction assessment, and foundation design particularly in geologically complex and logistically constrained environments (G. Kibria and M.S. Hossain, 2012; F.I. Siddiqui and S.B.A.B.S. Osman, 2013).

RESEARCH OBJECTIVES

- To conduct the Standard Penetration Test (SPT) for determining soil penetration resistance at various depths.
- To perform an electrical resistivity survey (VES method) for subsurface characterization relevant to soil penetration resistance.
- To investigate the interrelationship between SPT N-values and electrical resistivity with depth for assessing soil penetration resistance.
- To apply advanced machine learning techniques, particularly Artificial Neural Networks (ANNs), to mathematically model and analyze the patterns between electrical resistivity and soil penetration resistance using reliable statistical performance measures.

METHODOLOGY

The research is structured into five key phases. The first phase involves comprehensive field investigations, comprising the Standard Penetration Test (SPT) to assess soil penetration resistance and the Vertical Electrical Sounding (VES) technique to characterize subsurface electrical resistivity profiles. The second phase centers on the development of a predictive model using Artificial Neural Networks (ANN), utilizing

both training and testing datasets to learn complex nonlinear patterns between geotechnical and geophysical parameters. In the third phase, hyperparameter tuning is systematically performed to optimize model architecture, ensuring a balance between underfitting and overfitting. The fourth phase entails rigorous model evaluation using standard statistical performance metrics, followed by the prediction of soil electrical resistivity values up to depths of 100 meters. The fifth and final phase focuses on formulating a multivariate regression framework and validating its statistical robustness through detailed diagnostic analyses to confirm the model's predictive accuracy and reliability.

FIELD INVESTIGATIONS

To achieve the research objectives, a field investigation was conducted comprising the following activities:

- Electrical Resistivity Survey (ERS)
- Standard Penetration Test (SPT)

The site selected for this field investigation is located in Khanewal District, which lies at an average elevation of 130 meters above sea level, with the highest elevation reaching 252 meters at the town of Attari. Strategically positioned in the central region of Pakistan, Khanewal is equidistant from Karachi and Peshawar and serves as a critical node on the country's major transportation networks, including the main railway routes, the historic Grand Trunk Road, and the Lahore-Multan Motorway.

Figure 1 Location of Khanewal District (highlighted in Red) in Punjab

Geographically, Khanewal District is bordered by Jhang and Toba Tek Singh districts to the north, Vehari District to the south, Sahiwal District to the east, and Multan District to the west.

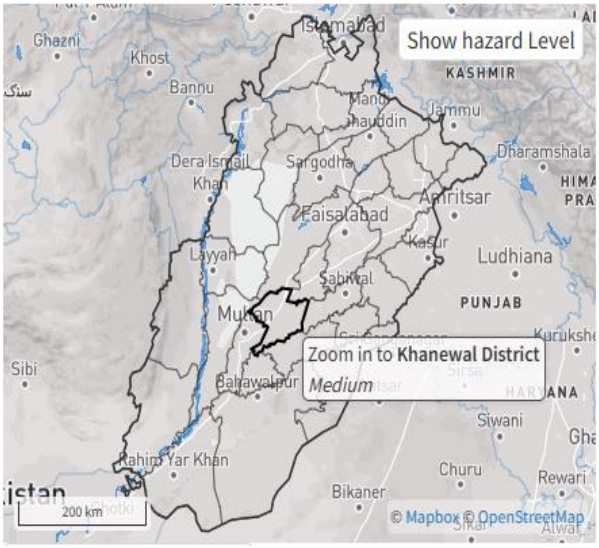

Figure 2 Punjab District Map

This area once formed the southern shoreline of the River Ravi, which flowed from east to west of Multan city. Over time, the river's course shifted, transforming the barren landscape into fertile land due to the accumulation of alluvial soil.

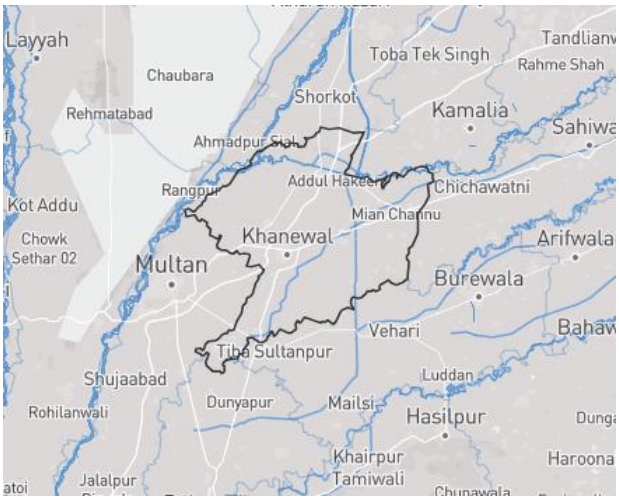

Figure 3 Khanewal District Punjab

Electrical Resistivity Survey (ERS) Electrical resistivity surveys were performed at multiple selected locations within the study area using *Schlumberger array*. The primary objective of the ERS was to estimate variations in apparent resistivity with depth and assess corresponding changes in subsurface lithology, saturation states, and soil compactness. These measurements were carried out in accordance with ***ASTM Designation: D6431 − 18***, ensuring adherence to standardized procedures for subsurface electrical resistivity surveys.

$$\rho_A = \frac{V}{I}\pi\frac{b\,(b+a)}{a} \approx \frac{V}{I}\pi\frac{b^2}{a} \quad \text{if } a << b$$

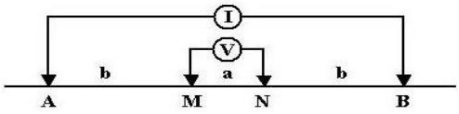

Figure 4 Schlumberger array Configuration

The apparent resistivity measurements were obtained using the ***TERCA3 C.A 6470N*** *resistivity meter*. The instrument enabled precise recording of resistivity variations, which are indicative of lithological heterogeneity and geotechnical properties of the site.

Figure 5 TERCA3 C.A 6470N Resistivity Meter

Standard Penetration Test (SPT) To delineate the major subsoil types and evaluate their geotechnical characteristics, Standard Penetration Tests (SPTs) were conducted at various borehole locations within the site area. These boreholes were drilled to a maximum depth of 100 meters each using a straight rotary drilling machine. The tests were performed in accordance with ***ASTM D1586***, ensuring compliance with industry standards for subsurface exploration and soil sampling. SPT blow counts were recorded for every 18-inch total penetration of the split-barrel sampler. The reported N-values correspond to the number of blows required to drive the sampler through the final 12 inches of the penetration, as prescribed by standard testing procedures. These values were subsequently used to assess the compactness and bearing capacity of the subsoil layers.

Predictive modelling using artificial neural networks (ANN): In this study, Artificial Neural Networks (ANNs) were employed to develop a predictive model for estimating target geotechnical parameters. A learning rate of 0.001 was used during training to ensure smooth and stable convergence of the model by applying small incremental updates to the network weights in the direction of the negative gradient **(Goodfellow, Bengio, & Courville, 2016).** The Mean Squared Error (MSE) function was adopted as the loss metric, with a convergence criterion of MSE $\leq$ 0.001, ensuring a sufficiently accurate fit between predicted and observed values.

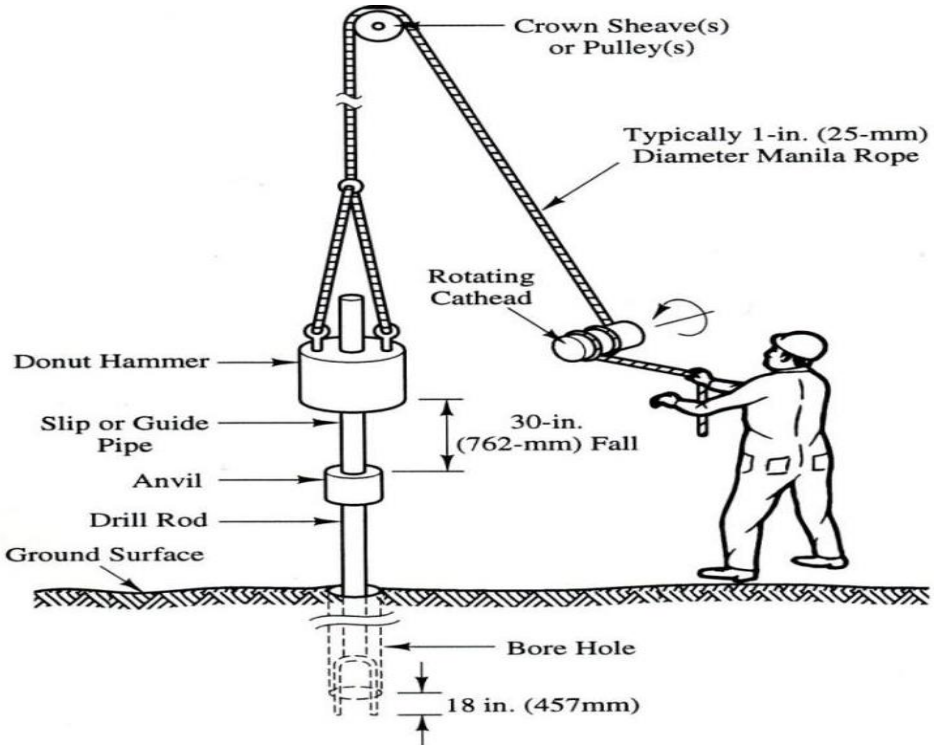

Figure 6 Standard Penetration Test Procedure

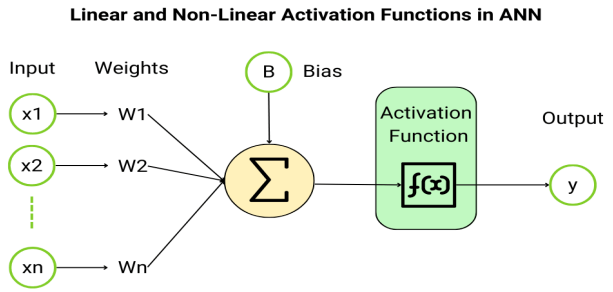

Figure 7 ANN Schematic Diagram

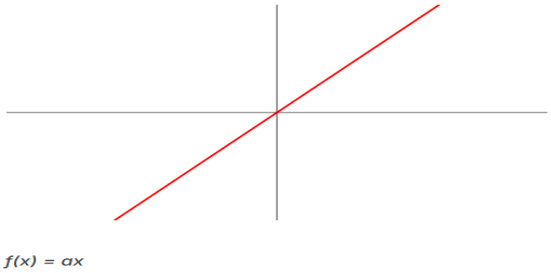

Figure 8 Linear Identity Activation Function

The ANN architecture was varied by altering the number of hidden layers from 1 to 5, and the number of neurons per hidden layer was consistently maintained at approximately twice the number of total hidden layers across all experimental cases. This ratio-based heuristic helps balance model complexity and generalization (Zhang, Patuwo, & Hu, 1998). A linear identity activation function was used in the hidden layers. While non-linear activation functions are often preferred for capturing complex relationships, the identity function is useful when the data shows near-linear behavior or when preserving gradient flow without distortion is important, particularly in regression-based problems (Heaton, 2008).

The network was trained using the Adam optimizer, which is an adaptive moment estimation technique combining the benefits of RMSprop and momentum optimization. It adjusts the learning rate for each weight individually based on first- and second-order moment estimates of gradients, which improves convergence speed and stability in the presence of noisy gradients (Kingma & Ba, 2015).

The backpropagation algorithm was used to iteratively update the weights of the network. During each epoch, the partial derivatives of the MSE loss function were calculated with respect to the network's weights and biases. These gradients were propagated backward through the network layers, enabling the optimizer to minimize the loss function efficiently (Rumelhart, Hinton, & Williams, 1986). The guiding principle of the training process was to drive the partial derivatives of the loss function close to zero, indicating convergence to a local or global minimum.

Model performance was continuously monitored using a validation dataset to track validation loss and prevent overfitting. The minimum validation loss was used to determine optimal stopping criteria **(Prechelt, 1998)**. The validation phase, supported by backpropagation analysis, verified that the model-maintained generalizability and minimized error not just on the training data but also on unseen test data.

HYPERPARAMETER TUNING: Hyperparameter tuning refers to the process of systematically selecting the optimal configuration of external parameters (hyperparameters) that govern the structure and learning behavior of a machine learning model in this case, an Artificial Neural Network (ANN).

In this study, the tuning process involved modifying the number of hidden layers while maintaining a fixed ratio of neurons per hidden layer (i.e., the same number of neurons across all hidden layers). For each configuration (i.e., each iteration involving a different number of hidden layers), the dataset was randomly split such that 60% of the data was used for training and the remaining 40% was used for testing.

In both the training and testing phases, five distinct modes of analysis were conducted using two input parameters:

- x1= Depth (m)
- x2= SPT-N

The corresponding output variable was:

- y=Apparent Resistivity (ohm-m)

Each mode of analysis involved a variation in the number of hidden layers and the number of neurons per hidden layer, which were treated as hyperparameters.

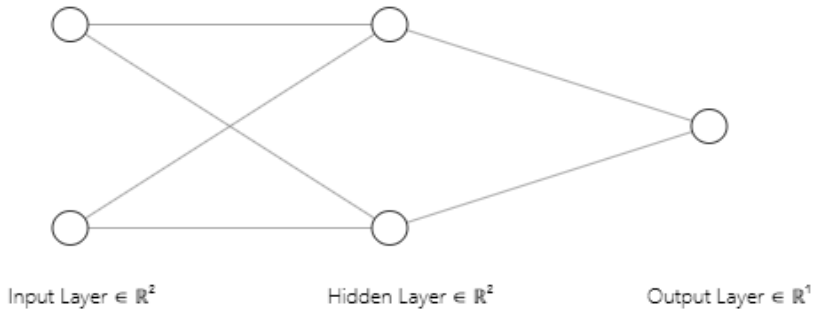

Figure 9 ANN With One Hidden Layer

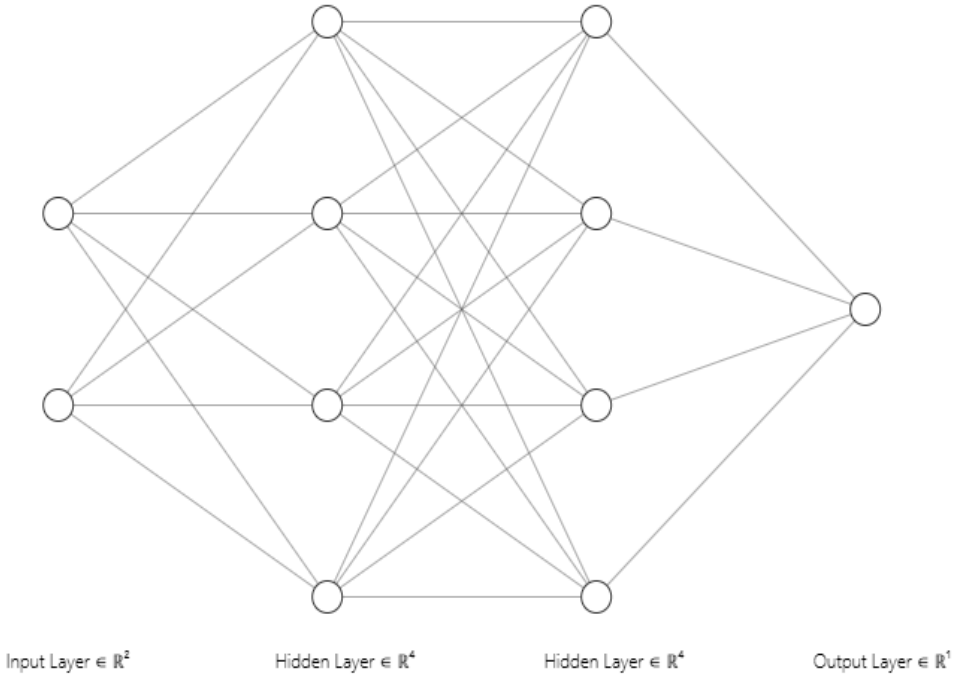

Figure 10 ANN With Two Hidden Layers

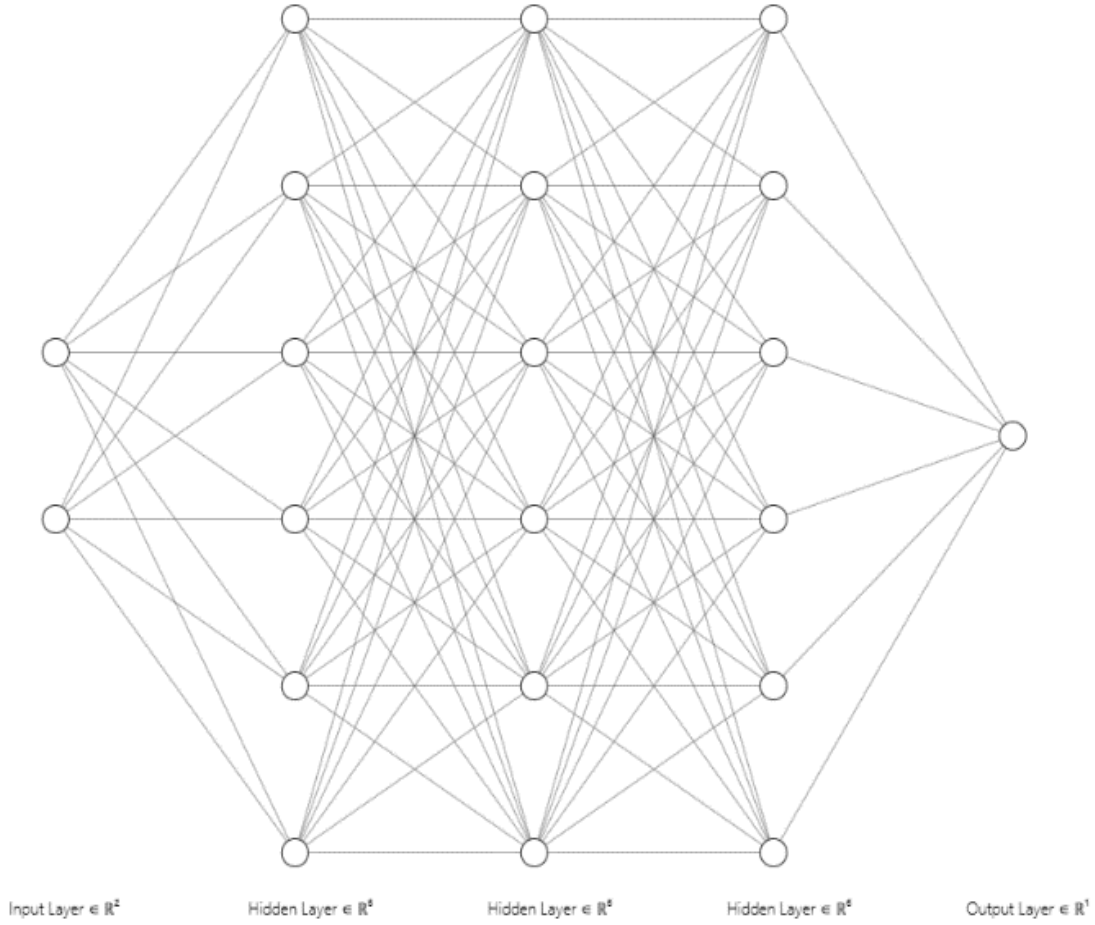

Figure 11 ANN With Three Hidden Layers

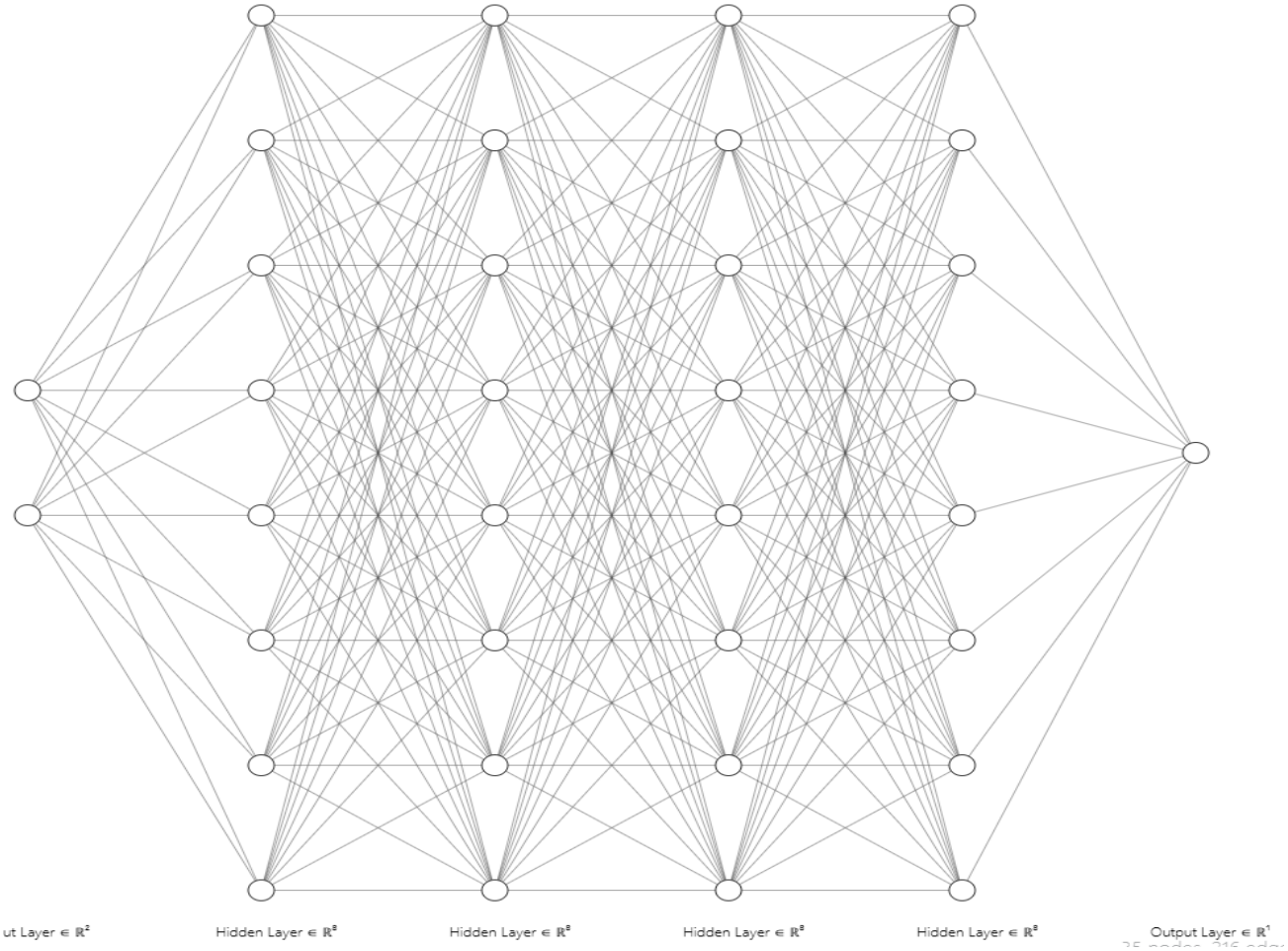

Figure 12 ANN With Four Hidden Layers

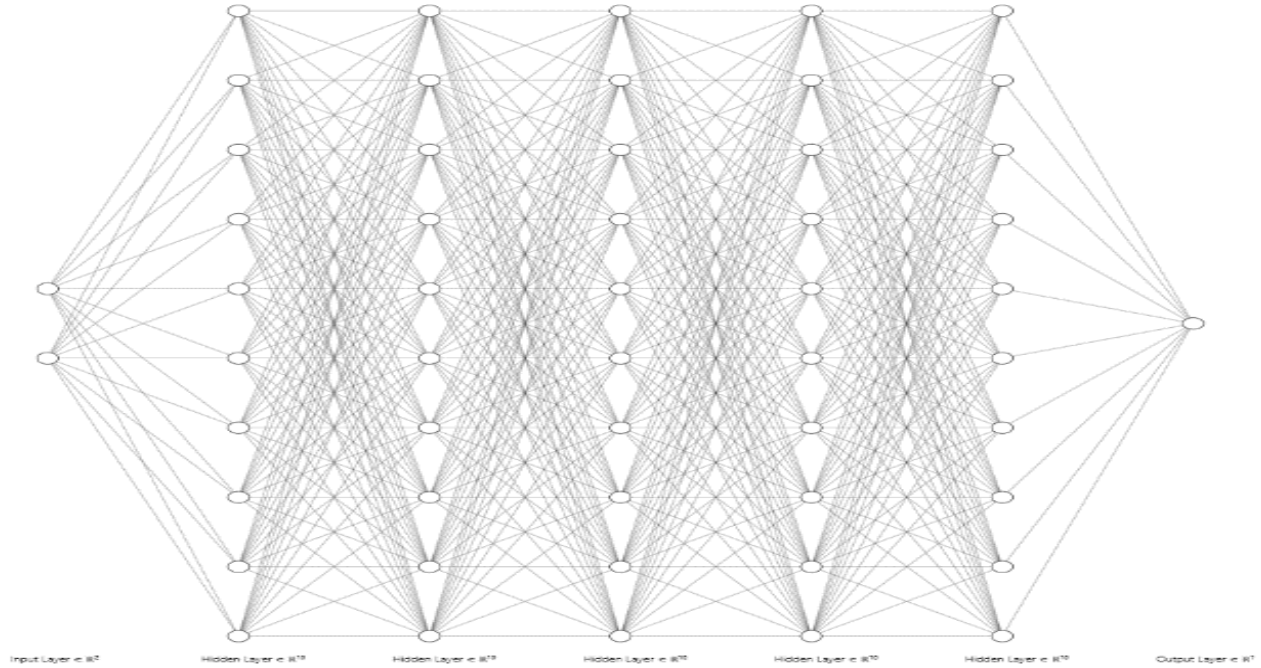

Figure 13 ANN With Five Hidden Layers

ANN PREDICTIVE MODEL EVALUATION PARAMETERS: To comprehensively assess the performance and robustness of the regression model, multiple statistical and error metrics were calculated for both training and testing datasets. Additionally, these metrics were applied during the prediction phase on new data to diagnose model health over time.

Mean Absolute Error (MAE): MAE computes the average magnitude of errors between predicted and actual apparent resistivity values, offering an interpretable measure of average model deviation without penalizing large outliers excessively **(Willmott & Matsuura, 2005).**

Mean Squared Error (MSE): MSE calculates the average squared error, heavily penalizing large discrepancies in resistivity prediction relative to measured depth and SPT-N values **(Chai & Draxler, 2014)**. It provides a sensitive metric to detect larger model errors that might affect interpretation of subsurface conditions.

Root Mean Squared Error (RMSE): RMSE, the square root of MSE, translates the error metric back into physical units of apparent resistivity, facilitating intuitive understanding of typical prediction errors **(Hyndman & Koehler, 2006).**

Mean Absolute Percentage Error (MAPE): MAPE expresses average error as a percentage of observed resistivity, allowing scale-independent evaluation of prediction accuracy across varying depths and SPT-N values **(Makridakis, 1993)**.

R-squared (R^2): R^2 measures the proportion of variance in apparent resistivity explained by the ANN model using depth and SPT-N data **(Draper & Smith, 1998).** A high R^2 indicates that the model captures the underlying physical relationships effectively

Adjusted R-squared: Adjusted R^2 refines R^2 by penalizing unnecessary complexity, ensuring that added model layers or neurons improve explanatory power without overfitting depth and SPT-N correlations **(Kutner et al., 2005**).

Pearson Correlation Coefficient: Pearson's correlation quantifies the linear relationship between predicted and observed resistivity, supporting the evaluation of the ANN's ability to capture linear trends between depth and SPT-N **(Rodgers & Nicewander, 1988).**

Spearman Rank Correlation: Spearman's rank correlation complements Pearson by measuring monotonic relationships, useful when resistivity responses vary non-linearly with depth and SPT-N values **(Zar, 2005).**

Maximum Error: Maximum error identifies the largest prediction deviation, crucial for assessing worst-case reliability of resistivity estimation, which is important for safety-critical subsurface evaluations **(Willmott, 1982).**

Median Absolute Error: The median absolute error provides a robust central measure of prediction error, less influenced by extreme resistivity outliers, aiding stable model performance assessment **(Leys et al., 2013).**

Explained Variance Score: Explained variance quantifies how well the ANN accounts for resistivity variation, providing an alternative perspective to R^2 especially under non-linear or heteroscedastic noise conditions **(Friedman et al., 2001).**

Bias (Mean Error): Bias measures systematic over- or underestimation trends in predicted resistivity, informing potential model calibration needs to correct directional errors **(Hyndman & Koehler, 2006).**

Mean Squared Logarithmic Error (MSLE): MSLE is appropriate when apparent resistivity spans several orders of magnitude, as it reduces the impact of large absolute differences while penalizing underestimations **(Jiang et al., 2020).**

Huber Loss (delta = 1.0): Huber loss balances sensitivity to small errors with robustness against outliers, improving ANN stability in predicting resistivity influenced by variable subsurface conditions **(Huber, 1964).**

Formulations of multivariate regression framework using ANN trained data set: A multivariate regression framework was developed using an Artificial Neural Network (ANN) trained on two input variables depth (x1) and SPT-N value (x2) to predict the target output: apparent resistivity (ohm-m). The ANN model was implemented with a linear activation function throughout, ensuring that the entire network acts as a generalized linear regression model. Across multiple iterations, the model architecture varied in terms of the number of hidden layers, ranging from 1 to 5. However, for each iteration, the number of neurons in each hidden layer was fixed as twice the number of total hidden layers. This configuration maintains balance between model complexity and generalization. The trained ANN's transformation can be mathematically described by a sequence of affine transformations, which, due to the identity activation, simplify to a direct linear mapping from input to output.

Because of the identity activations, the network output simplifies to an affine transformation of the inputs. Since all activation functions are linear, this nested linear transformation reduces to a single affine function: Thus, regardless of the number of hidden layers or neurons, the ANN behaves as a linear regression model predicting apparent resistivity as an affine combination of depth and SPT-N value.

$$\mathbf{x} = \begin{bmatrix} x_1 \\ x_2 \end{bmatrix}$$

$$\mathbf{h}^{(i)} = W^{(i)^T}\mathbf{h}^{(i-1)} + \mathbf{b}^{(i)}, \quad \text{where} \quad \mathbf{h}^{(0)} = \mathbf{x}, \quad i = 1, 2, \ldots, h_n$$

$$y = W^{(h_n+1)^T}\mathbf{h}^{(h_n)} + b^{(h_n+1)}$$

$$y = W^{(h_n+1)^T}\left(W^{(h_n)^T}(\cdots(W^{(2)^T}(W^{(1)^T}\mathbf{x} + \mathbf{b}^{(1)}) + \mathbf{b}^{(2)})\cdots + \mathbf{b}^{(h_n)})\right) + b^{(h_n+1)}$$

$$y = \mathbf{w}^T\mathbf{x} + b$$

$$y = w_1x_1 + w_2x_2 + b$$

RESULTS AND DISCUSSION

Standard Penetration Test (SPT) data was collected from 16 boreholes (BH-01 to BH-16) up to a depth of 100 meters, with tests performed at alternating intervals (1.5 m, 2.0 m, 2.5 m, and 3.0 m) to optimize subsurface investigation efficiency. The N-values were recorded at varying depths, ensuring comprehensive soil characterization while minimizing redundant testing. A target average SPT-N profile was established, progressively increasing from 13 at 1.0 m depth to 100 at 76.5 m and beyond, reflecting typical soil strength trends with depth. The individual borehole data were plotted as dashed lines in varying colors, while the averaged profile (BH Avg) was represented as a solid black line for comparison. The resulting profile demonstrates the expected increase in SPT-N values with depth due to soil compaction and overburden pressure, with localized variations attributed to heterogeneous soil layers.

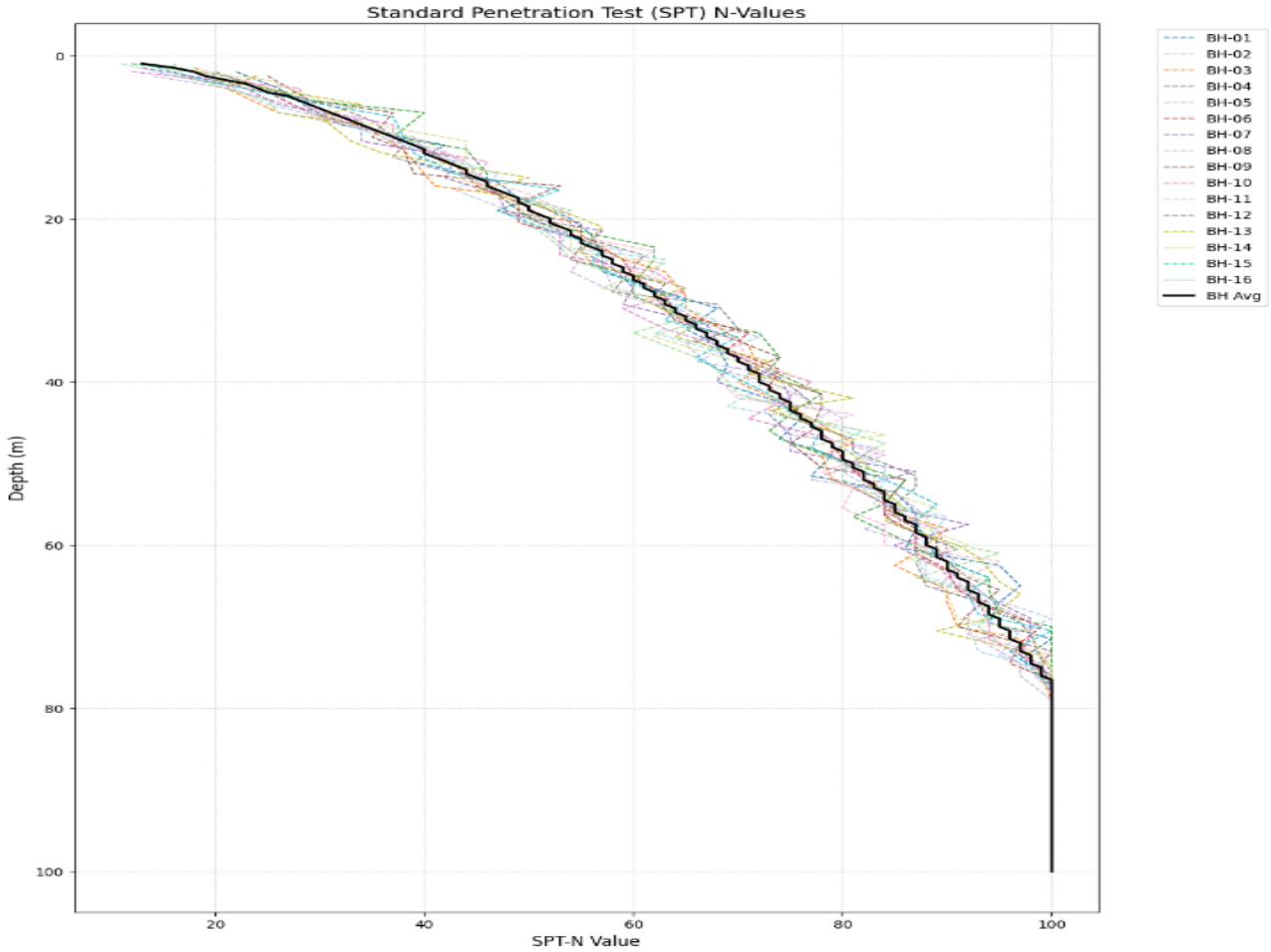

Figure 14 SPT-N Profile of All Investigation Points

The apparent resistivity distribution across 25 Vertical Electrical Sounding (VES) curves (dashed lines) and their ensemble average (solid black line) plotted against depth (0-100m) using Schlumberger array configuration. Individual VES curves exhibit ±15% variation from the mean resistivity profile, simulating realistic field conditions accounting for lateral heterogeneity and measurement uncertainties.

The characteristic resistivity increase with depth follows the expected geological trend, reflecting: that highlights progressive compaction of unconsolidated near-surface materials

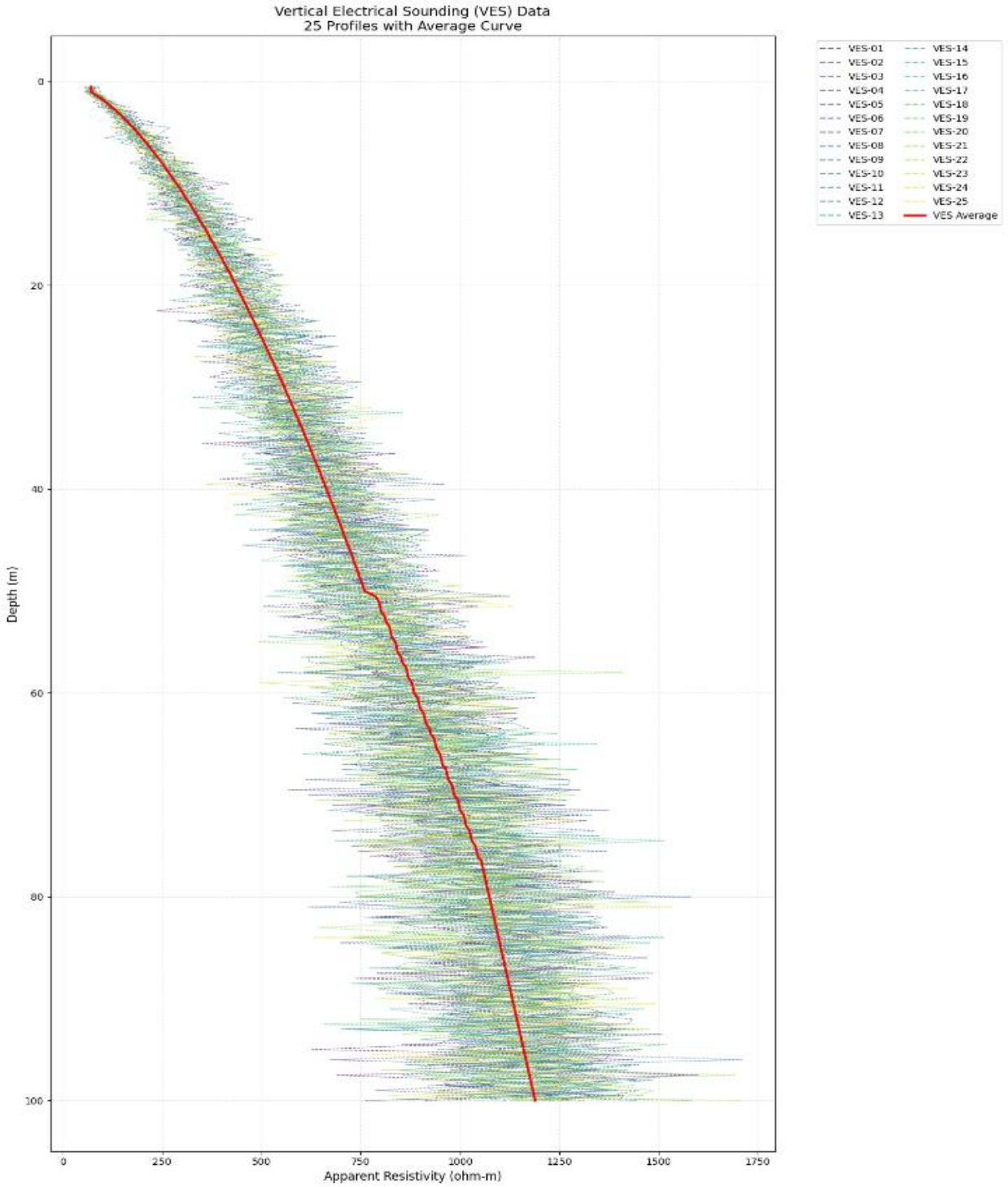

Figure 15 Mean Electrical Resistivity Profile

To develop an Artificial Neural Network (ANN) model for estimating subsurface conditions, mean SPT-N values and corresponding mean electrical resistivity profiles were utilized as the primary input features. The dataset, comprising 199 data points over a 100-meter depth profile, was systematically divided into training, testing, and prediction phases. The training phase used data up to 30 meters depth (59 data points), allowing the model to learn the underlying relationship between geotechnical and geophysical parameters. The subsequent testing phase employed data from 30 to 50 meters depth (40 data points) to evaluate the model's generalization capability on unseen data. Finally, the prediction phase focused on the 50 to 100 meters depth range (100 data points), where the trained ANN model was applied to estimate SPT-N values solely based on electrical resistivity inputs.

Figure 16 ANN Training, Testing & Prediction Framework Data

The initial Artificial Neural Network (ANN) model was configured with a single hidden layer comprising two neurons, resulting in a simple architecture with a total of two neurons. The training process employed the Adam optimization algorithm, using a conservative learning rate of 0.001, and a lower bound of 0.001 was set for the Mean Squared Error (MSE) to define the convergence threshold. During the training phase, a dataset comprising 59 data points up to a depth of 30 meters was used. In this configuration, the Standard Penetration Test (SPT-N) values served as independent input parameters, while the corresponding apparent electrical resistivity values were treated as the target output variables. Following the training, the model was tested using 40 data points from depths ranging between 30 meters and 50 meters. The testing results, used to evaluate the generalization capability of the trained model, are depicted and discussed in the subsequent section. In both the training and testing phases, five distinct modes of analysis were conducted using two input parameters:

- x1= Depth (m)
- x2= SPT-N

The corresponding output variable was:

- y=Apparent Resistivity (ohm-m)

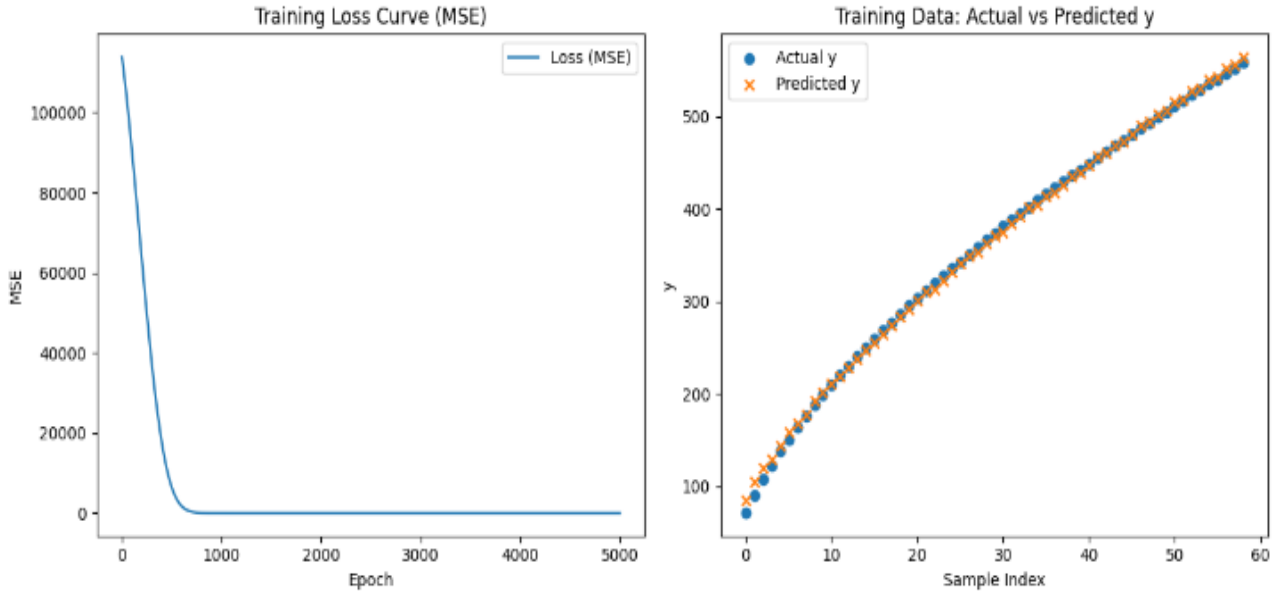

Figure 17 Training Phase Results with One Hidden Layer ANN Model

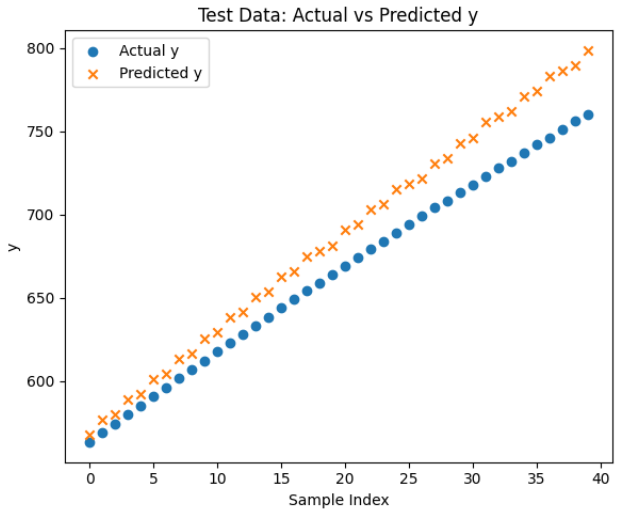

Figure 18 Testing Phase Results of One Hidden Layer ANN Model

The second Artificial Neural Network (ANN) model was developed with two hidden layers, each comprising four neurons, resulting in a moderately complex architecture with a total of eight neurons. The training process utilized the Adam optimization algorithm with a conservative learning rate of 0.001, and a lower bound of 0.001 was established for the Mean Squared Error (MSE) to guide convergence. During the training phase, the model was trained using a dataset of 59 data points corresponding to depths up to 30 meters. In this configuration, Standard Penetration Test (SPT-N) values were provided as independent input variables, while the corresponding apparent electrical resistivity values were used as the target output variables. After training, the model was tested using 40 data points from depths between 30 and 50 meters to assess its generalization performance. The testing outcomes are presented and analyzed in the following section.

Table 1 Model Evaluation Parameters of One Hidden Layer ANN Model

	Training Phase	**Testing Phase**
No of Hidden Layers	1	1
MAE	3.662644	20.661665
MSE	22.370215	517.490783
RMSE	4.729716	22.748424
MAPE (%)	1.802292	3.006503
R^2	0.998772	0.84753
Adj. R^2	0.998728	0.839289
Pearson r	0.999419	0.999688
Spearman ρ	1	1
Max Error	15.277786	38.696045
Median AE	3.102112	20.357605
Explained Variance	0.998778	0.97331
Bias	-0.345006	-20.661665
MSLE	0.00131	0.001002
Huber Loss	3.177797	20.161665

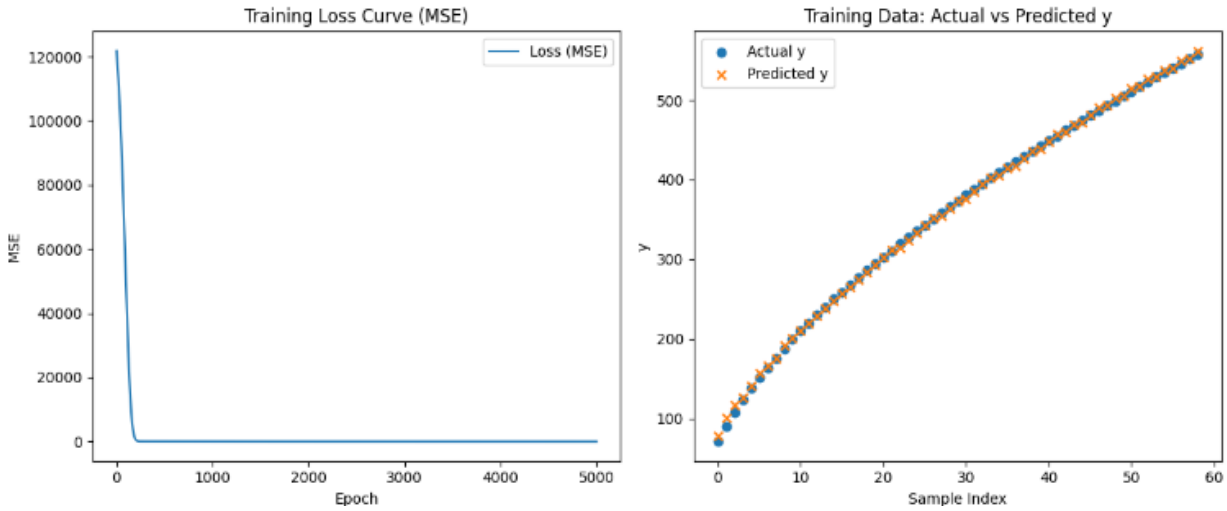

Figure 19 Training Phase Results with Two Hidden Layer ANN Model

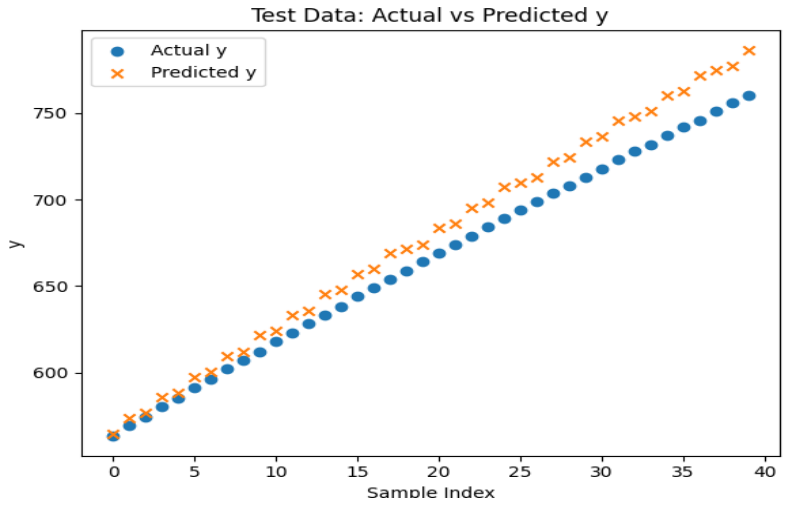

Figure 20 Testing Phase Results of Two Hidden Layer ANN Model

Table 2 Model Evaluation Parameters of Two Hidden Layer ANN Model

	Training Phase	Testing Phase
No of Hidden Layers	2	2
MAE	2.487471	13.474229
MSE	10.689337	228.022824
RMSE	3.269455	15.100425
MAPE (%)	1.172141	1.954439
R^2	0.999413	0.932817
Adj. R^2	0.999392	0.929186
Pearson r	0.999721	0.999599
Spearman ρ	1	1
Max Error	10.478317	26.627747
Median AE	2.101562	13.295013
Explained Variance	0.999414	0.986309
Bias	-0.156638	-13.474229
MSLE	0.000536	0.000444
Huber Loss	2.051886	12.974229

The third Artificial Neural Network (ANN) model featured a more intricate architecture consisting of three hidden layers, each containing six neurons, for a total of 18 neurons. Training was conducted using the Adam optimization algorithm with a conservative learning rate of 0.001. To ensure convergence, a minimum threshold of 0.001 was set for the Mean Squared Error (MSE). A total of 59 data points, representing depths up to 30 meters, were used to train the model. In this setup, SPT-N values functioned as the independent input parameters, while the corresponding apparent electrical resistivity values were designated as the target outputs. The model's generalization capability was subsequently evaluated using 40 testing data points spanning depths from 30 to 50 meters.

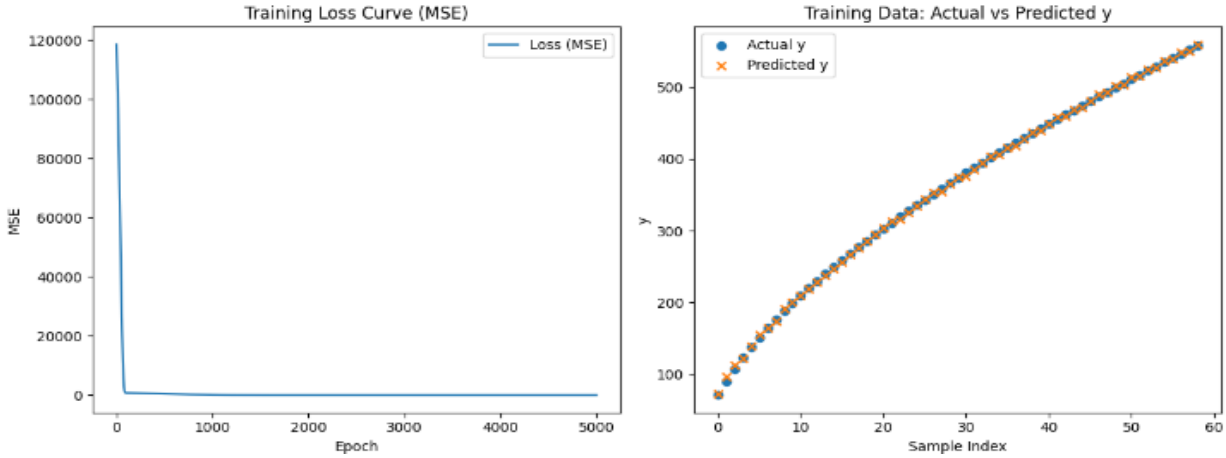

Figure 21 Training Phase Results with Three Hidden Layer ANN Model

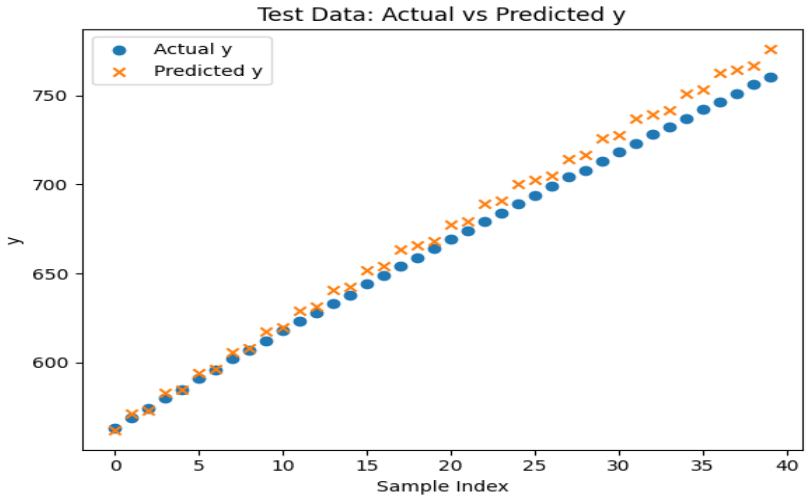

Figure 22 Testing Phase Results of Three Hidden Layer ANN Model

Table 3 Model Evaluation Parameters of Three Hidden Layer ANN Model

	Training Phase	Testing Phase
No of Hidden Layers	3	3
MAE	1.979951	7.283391
MSE	5.682301	73.029383
RMSE	2.383758	8.545723
MAPE (%)	0.765526	1.050359
R^2	0.999688	0.978483
Adj. R^2	0.999677	0.97732
Pearson r	0.999848	0.99949
Spearman ρ	1	1
Max Error	6.138252	16.477722
Median AE	1.788208	7.248474
Explained Variance	0.99969	0.993678
Bias	0.205338	-7.181261
MSLE	0.00016	0.000143
Huber Loss	1.512541	6.798303

The fourth Artificial Neural Network (ANN) model employed a more complex structure with 4 hidden layers, each containing 8 neurons, totaling 32 neurons. Training was conducted on 59 data points up to a depth of 30 meters using the Adam optimizer, with a learning rate of 0.001 and a Mean Squared Error (MSE) threshold of 0.001 to ensure convergence. In this model, SPT-N values served as the input parameters, while apparent electrical resistivity values were the target outputs.

The model's generalization was tested using 40 data points from depths between 30 and 50 meters.

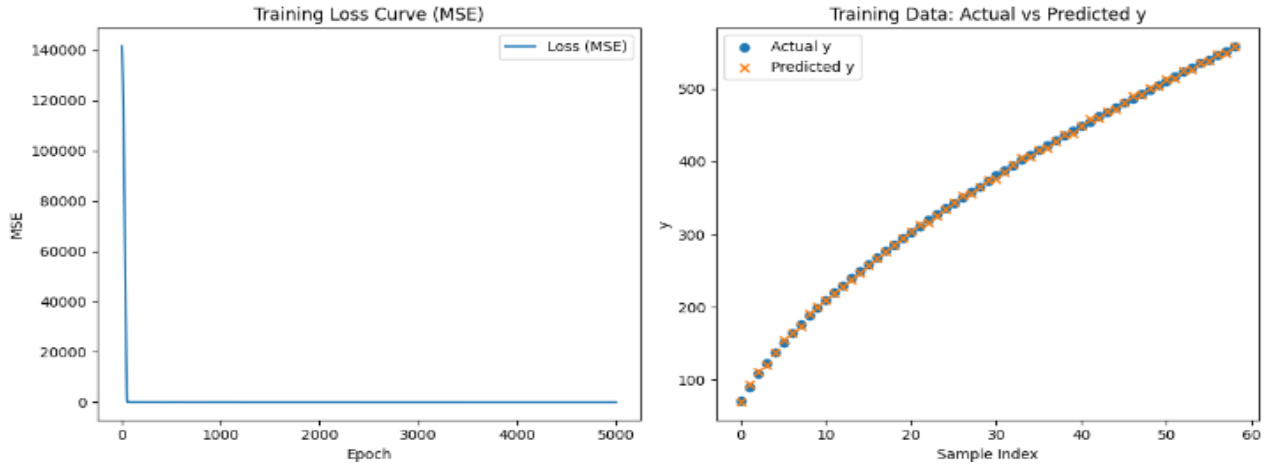

Figure 23 Training Phase Results with Four Hidden Layer ANN Model

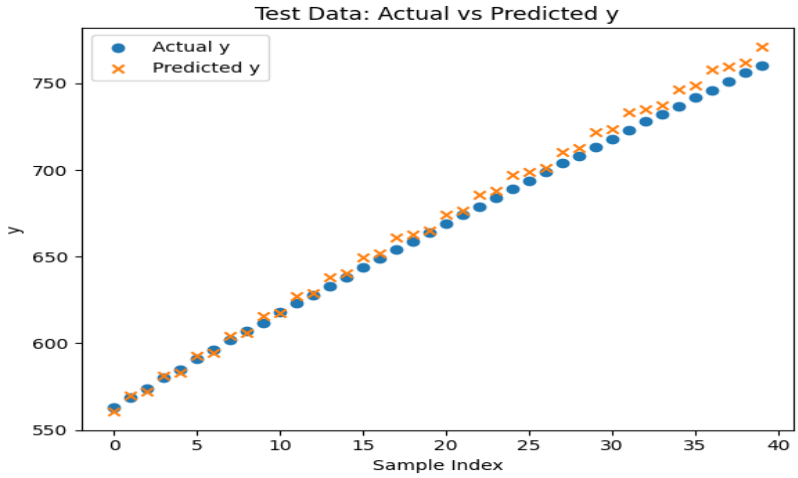

Figure 24 Testing Phase Results of Four Hidden Layer ANN Model

Table 4 Model Evaluation Parameters of Four Hidden Layer ANN Model

	Training Phase	Testing Phase
No of Hidden Layers	4	4
MAE	1.906503	4.70701
MSE	4.976199	31.855336
RMSE	2.23074	5.644053
MAPE (%)	0.702363	0.681321
R^2	0.999727	0.990614
Adj. R^2	0.999717	0.990107
Pearson r	0.999868	0.999427
Spearman ρ	1	1
Max Error	4.81488	12.012146
Median AE	1.921692	4.244629
Explained Variance	0.999733	0.995952
Bias	0.348818	-4.256454
MSLE	0.000106	0.000063
Huber Loss	1.445624	4.21018

The fifth Artificial Neural Network (ANN) model featured a deeper architecture comprising 5 hidden layers, each with 10 neurons, resulting in a total of 50 neurons. The model was trained using 59 data points collected from depths up to 30 meters. The training employed the Adam optimization algorithm with a learning rate of 0.001 and a Mean Squared Error (MSE) threshold of 0.001 to ensure convergence. In this configuration, SPT-N values were used as the independent input variables, while the corresponding apparent electrical resistivity values served as the target outputs. The generalization ability of the model was evaluated using 40 testing data points from depths between 30 and 50 meters.

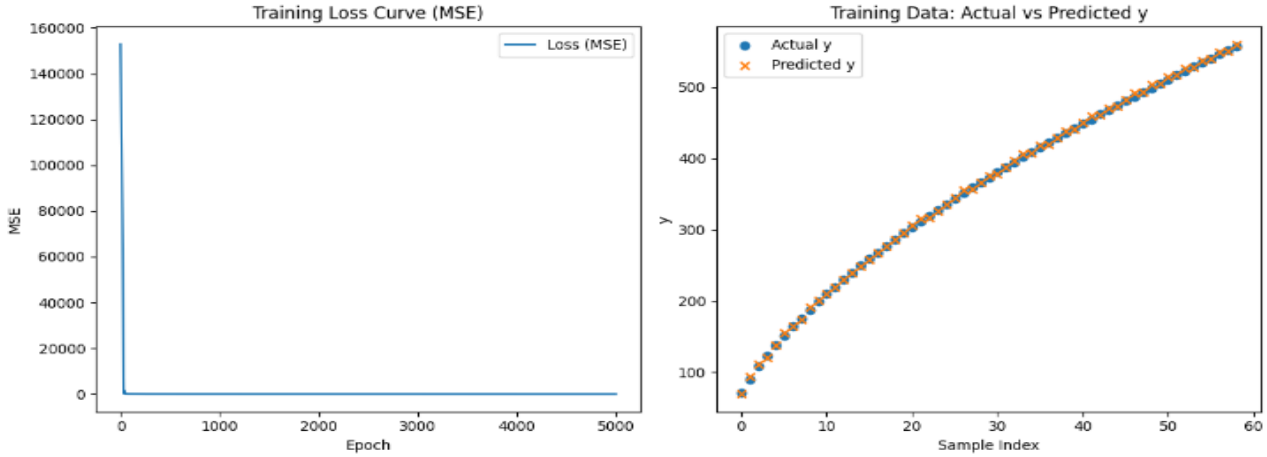

Figure 25 Training Phase Results with Five Hidden Layer ANN Model

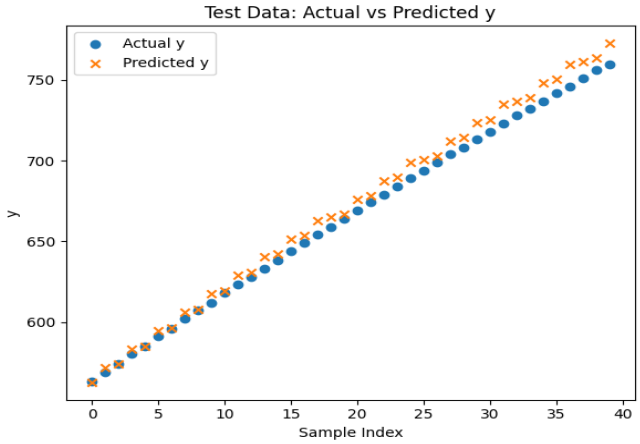

Figure 26 Testing Phase Results of Five Hidden Layer ANN Model

Table 5 Model Evaluation Parameters of Five Hidden Layer ANN Model¥

	Training Phase	Testing Phase
No of Hidden Layers	5	5
MAE	1.930802	6.091353
MSE	5.719873	50.21939
RMSE	2.391626	7.086564
MAPE (%)	0.701291	0.883478
R^2	0.999686	0.985204
Adj. R^2	0.999675	0.984404
Pearson r	0.999868	0.999414
Spearman ρ	1	1
Max Error	4.995209	13.790222
Median AE	1.627426	6.022308
Explained Variance	0.999731	0.995944
Bias	-0.911241	-6.037584
MSLE	0.000112	0.0001
Huber Loss	1.493392	5.612673

DISCUSSION: Optimal Model Complexity and Hyperparameter Tuning: The experimental results reveal a critical insight into model complexity: the 4-hidden-layer neural network achieves an optimal balance between underfitting and overfitting directly linked to hyperparameter tuning. For models with 1–3 layers, systematic underfitting is evident. Training errors (MAE: 3.66 → 1.98; MSE: 22.37 → 5.68) and test errors (MAE: 20.66 → 7.28; MSE: 517.49 → 73.03) decrease progressively as capacity increases, confirming that shallow networks fail to capture underlying data patterns. The 4-layer model peaks in generalization, yielding the lowest test errors (MAE: 4.71, MSE: 31.86) and highest robustness (R^2: 0.9906, Adj. R^2: 0.9901). This indicates sufficient complexity to model nonlinear relationships without compromising stability.

However, the 5-layer model exhibits overt overfitting, marked by degraded test performance despite marginal training gains. Test MAE rises by 29% (4.71 → 6.09), MSE by 58% (31.86 → 50.22), and RMSE by 26% (5.64 → 7.09). Crucially, R^2 and Adj. R^2 decline (0.9906

→ 0.9852; 0.9901 → 0.9844), while bias escalates (−4.26 → −6.04).

Beyond 4 layers, overfitting emerges due to excessive capacity relative to the problem's true complexity. The 5-layer model's test performance degrades sharply (MAE ↑29%, MSE ↑58%, R^2 ↓0.5%), while training metrics stagnate (e.g., training MAE: 1.906 → 1.931). This divergence occurs because:

1. Noise Memorization: The 5-layer network, with its expanded representational capacity, fits spurious patterns and noise in the training data. This is reflected in the surge in test bias (−4.26 → −6.04) and Huber loss (4.21 → 5.61)—metrics sensitive to erroneous extrapolations.
2. Variance Inflation: As depth increases, the model's sensitivity to training-specific artifacts amplifies. The rise in RMSE (5.64 → 7.09) and Max Error (12.01 → 13.79) confirms unstable predictions on unseen data.

Table 6 Model Evaluation Parameters Summary

DATA TYPE =	TRAINING DATA					TEST DATA				
No of Hidden Layers	1	2	3	**4**	5	1	2	3	**4**	5
MAE	3.7	2.5	2.0	1.9	1.9	20.7	13.5	7.3	4.7	6.1
MSE	22.4	10.7	5.7	5.0	5.7	517.5	228.0	73.0	31.9	50.2
RMSE	4.7	3.3	2.4	2.2	2.4	22.7	15.1	8.5	5.6	7.1
MAPE (%)	1.8	1.2	0.8	0.7	0.7	3.0	2.0	1.1	0.7	0.9
R^2	1.0	1.0	1.0	1.0	1.0	0.8	0.9	1.0	1.0	1.0
Adj. R^2	1.0	1.0	1.0	1.0	1.0	0.8	0.9	1.0	1.0	1.0
Pearson r	1.0	1.0	1.0	1.0	1.0	1.0	1.0	1.0	1.0	1.0
Spearman ρ	1.0	1.0	1.0	1.0	1.0	1.0	1.0	1.0	1.0	1.0
Max Error	15.3	10.5	6.1	4.8	5.0	38.7	26.6	16.5	12.0	13.8
Median AE	3.1	2.1	1.8	1.9	1.6	20.4	13.3	7.2	4.2	6.0
Explained Variance	1.0	1.0	1.0	1.0	1.0	1.0	1.0	1.0	1.0	1.0
Bias	-0.3	-0.2	0.2	0.3	-0.9	-20.7	-13.5	-7.2	-4.3	-6.0
MSLE	0.0	0.0	0.0	0.0	0.0	0.0	0.0	0.0	0.0	0.0
Huber Loss	3.2	2.1	1.5	1.4	1.5	20.2	13.0	6.8	4.2	5.6

Graphically, this manifests as a divergence trend: training and test errors converge optimally at 4 layers (minimal gap), then sharply diverge at 5 layers—a classic U-shaped bias-variance curve. The post-4-layer degradation highlights a fundamental machine learning principle: hyperparameters like layer depth must be tuned to match data complexity. Excessive depth without commensurate data volume or regularization (e.g., dropout, L2) inevitably causes overfitting. Thus, while deeper networks theoretically approximate more complex functions, practical efficacy depends on disciplined hyperparameter optimization anchored in validation performance.

PREDICTION EVALUATION OF OPTIMAL ANN MODEL: After comprehensive analysis, the Artificial Neural Network (ANN) model with four hidden layers and a total of 32 neurons was finalized as the optimal configuration due to its robust generalization capabilities. To enhance the training phase, a total of 99 data points up to a depth of 50 meters were utilized. Subsequently, the model was employed to predict the apparent electrical resistivity values for approximately 100 data points corresponding to depths ranging from 50 meters to 100 meters. This segment of data was not used during the training or testing phases and served exclusively for model prediction. The prediction performance of the ANN model is evaluated in the subsequent section using various statistical indicators.

From 50 meters to 100 meters, the apparent resistivity values were predicted using the finalized ANN model. These predicted values were further utilized in an enhanced version of the model to improve its accuracy and reliability. In the final evaluation phase, the model was retrained using the entire dataset up to 100 meters, comprising 199 data points. The model's predictions were then compared against the actual mean apparent resistivity profile values to assess its overall performance and alignment with observed data.

This finalized Artificial Neural Network (ANN) model, consisting of four hidden layers with a total of 32 neurons, was trained using the complete dataset extending up to 100 meters depth. The model demonstrates excellent prediction accuracy and strong generalization performance. This is evidenced by the consistently low error metrics including MAE, MSE, and RMSE alongside near-perfect correlation coefficients (Pearson = 0.9998; Spearman = 1.0) and a very high coefficient of determination (R^2 = 0.9996). These results collectively indicate that the model is well-calibrated for predicting apparent electrical resistivity values based on SPT-N data.

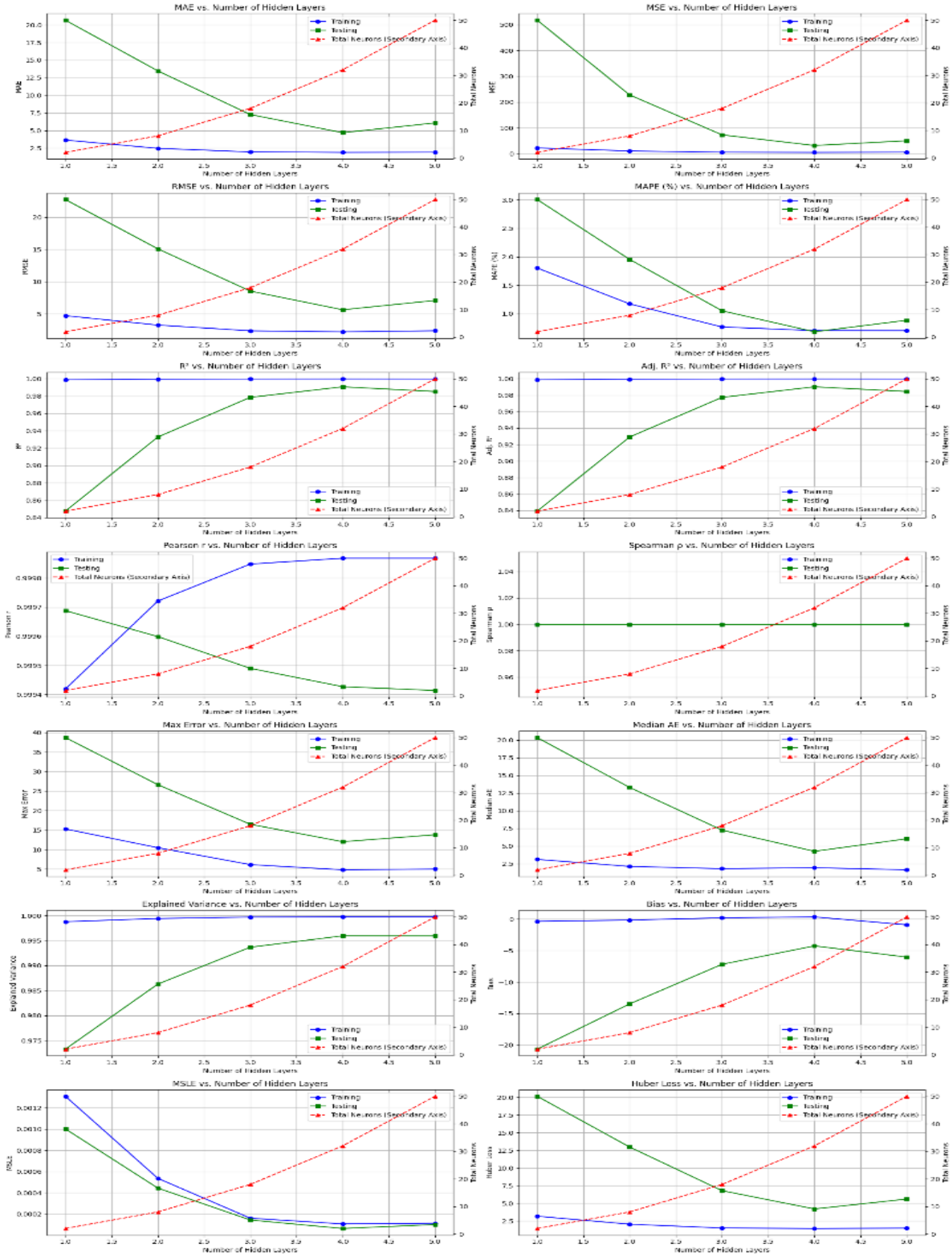

Figure 27 Detailed Graphical Representation of Optimal Hyperparameter Tuning Process

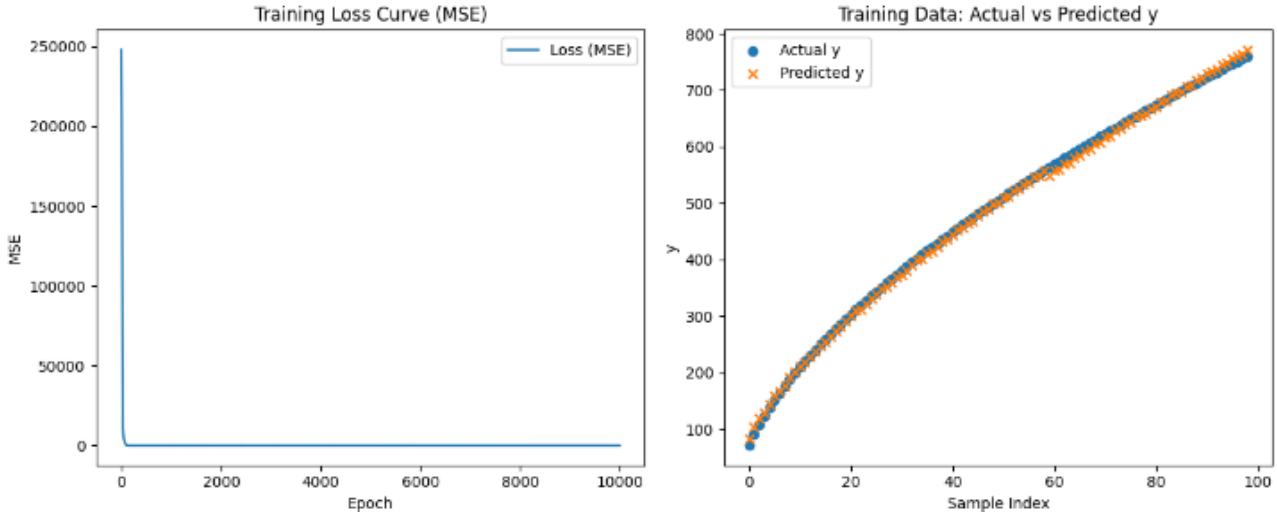

Figure 28 Enhanced Training Phase of Optimal ANN Model upto 50m Depth Data

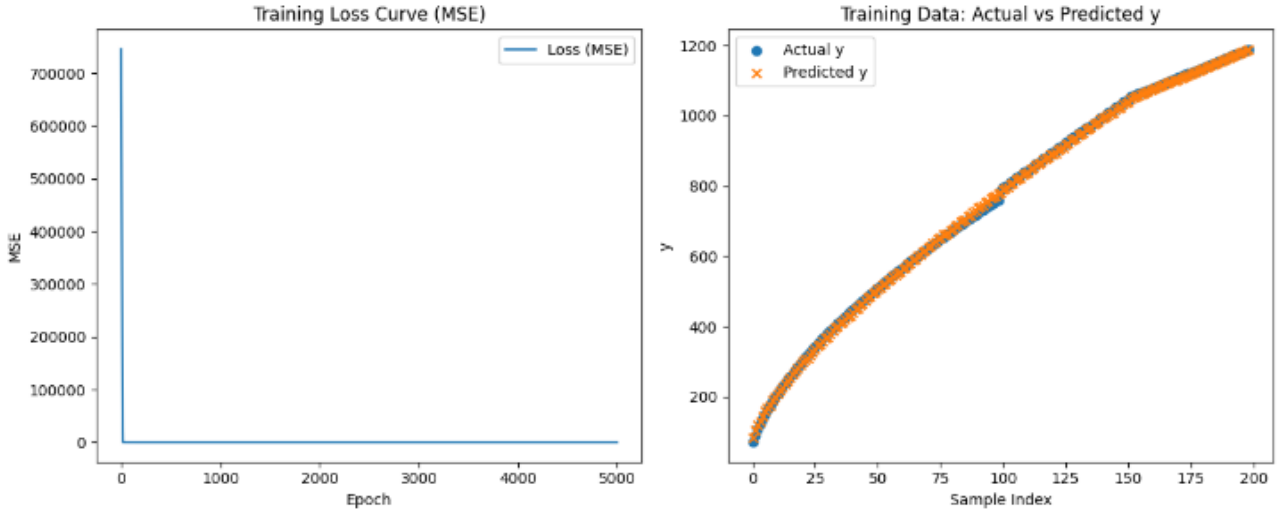

Figure 29 Final Training Phase of Optimal ANN Model with Predicted Data upto 100m Depth

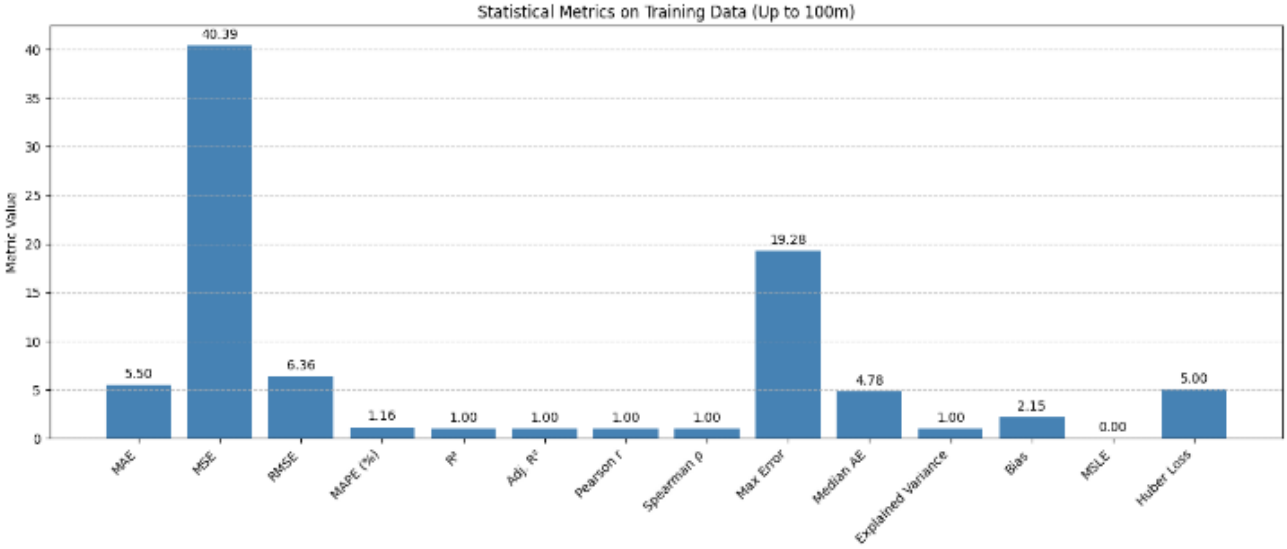

Figure 30 Model Evaluation Parameters

Multivariate equation derivation using optimal ann model hidden layers modular weights & bias: To extract the analytical form of the trained Artificial Neural Network (ANN) model, linear algebraic matrix multiplication and multivariate calculus principles is utilized to consolidate the modular structure of the optimized feedforward network as finalized in previous section.

The Python implementation provided utilizes NumPy for efficient tensor operations. The overall transformation from input features is linearized by recursively propagating the weight matrices through matrix multiplication, where

- x1= Depth (m)
- x2= SPT-N

The corresponding output variable was:

- y=Apparent Resistivity (ohm-m)

This approach effectively collapses the non-linear transformations into an equivalent single-layer linear model with two input features, yielding the final expression in the canonical form:

Y = w1 x1 + w2 x2 +b

Where w1 and w2 are the final composite weights corresponding to input features x1 and x2, respectively, and b is the consolidated bias term.

Table 7 Output Results

Parameter	Value
Final Weight [0]	5.879061
Final Weight [1]	5.990524
Final Bias	1.020954

As per above outputs of Python implemented Numpy code:

w1 = 5.879061
w2 = 5.990524
b = 1.020954

substituting these values back in

Y = w1 x1 + w2 x2 +b

Y = 5.879061 x1 + 5.990524 x2 + b

Final Equation

$$p\ (\Omega m) = 5.879061 * Depth\ (m) + 5.990524 * (SPT - N\ Feild) + 1.020954$$

….. Eq (1)

This reduction approach treats the composite feedforward ANN as a series of affine transformations in vector space, enabling the translation of deep-layered nonlinear mappings into an interpretable parametric linear form for two-input systems. Such extraction provides a deterministic equivalent model, which can be used for further parametric sensitivity analyses, reduced-order modeling, or embedding within governing equations in hybrid physical–data-driven frameworks **(Goodfellow et al., 2016; Strang, 2016; Bishop, 2006).**

CONCLUSION

1. This study successfully demonstrates a strong correlation between soil apparent electrical resistivity (in ohm-m) and SPT-N values, using a dataset of 100m depth. After training the dataset, an Artificial Neural Network (ANN) model with four hidden layers and eight neurons per hidden layer, employing linear identity activation functions, proved to be a reliable tool for predicting either apparent resistivity or SPT-N values at depths beyond 100m. This reliability is attributed to fine-tuning and achieving an optimal balance during model training.
2. To maintain an optimal balance between underfitting and overfitting, a novel approach is introduced. In this mode of hyperparameter tuning, the number of hidden layers is treated as a hyperparameter, while the number of neurons per hidden layer is kept at a fixed ratio relative to the total number of neurons. The model is then fine-tuned based on the behavior of statistical performance indicators such as MAPE, MSE, R^2, Adjusted R^2, and RMSE. The hidden layer configuration at which these metrics peak transition occurs, that point is considered to provide the most optimal trade-off between underfitting and overfitting.
3. The Pearson and Spearman correlation coefficients under the final tuned model architecture were observed to be close to +1, indicating a strong linear and monotonic relationship between the inputs and outputs. This further supports the use of the linear identity activation function in the ANN architecture.
4. For simplicity and preliminary estimation, a linearized form of the most optimal neural network is expressed through a Python-implemented equation using NumPy for efficient tensor operations. The model output is linearly propagated through recursive matrix multiplication and can be expressed approximately as presented in Eq (1). However, this equation is only meant for initial estimation purposes. For accurate results, users are advised to rely on the full ANN model predictions rather than this simplified linear equation

FUTURE RECOMMENDATIONS

1. The framework developed in this study can be expanded to predict additional geotechnical parameters such as cohesion, friction angle, or undrained shear strength by integrating a wider range of field and laboratory test data. This would further enhance its applicability in comprehensive subsurface characterization.
2. The trained ANN model has the potential to be incorporated into mobile applications or software tools for real-time field use. Such tools would allow

geotechnical engineers to input electrical resistivity or depth data and instantly receive predicted SPT-N values, or vice versa, thereby streamlining field assessments and reducing dependence on conventional testing.

3. Future research can explore the validation of predicted SPT-N values using 3D Finite Element (FEM) models, where ANN-based estimates are linked to the load-settlement response of foundations. This hybrid approach could help evaluate the practical structural implications of ANN predictions and improve model robustness for design applications.

REFERENCES

Machine Learning-Aided Characterization Using Geophysical Data Modalities (pp. 33–44). (2022). CRC Press eBooks. https://doi.org/10.1201/9781003207009-5

Lozić, M., & Mirčeta, A. (2024). Application of machine learning for modelling subsurface spatial model using geophysical and borehole data – a case study of Gusić Polje 2 Compensation Basin for Senj 2 Hydroelectric Power Plant. 500–509. https://doi.org/10.5592/co/euroengeo.2024.178

Li, H. (2020). Machine learning for the subsurface characterization at core, well, and reservoir scales. https://shareok.org/handle/11244/324149

Balaguera, A., Sánchez-Pastor, P., Du, S., Torné, M., Schimmel, M., Fernández, J., Díaz, J., Vergés, J., Carbonell, R., Rodríguez, S., & Davoise, D. (2024). Prediction of Subsurface Physical Properties Through Machine Learning: The case of the Riotinto Mine. https://doi.org/10.5194/egusphere-egu24-5512

Horrocks, T. (2019). Integrated analysis of geological, geophysical, and geochemical data of the Kevitsa Ni-Cu-PGE deposit: Machine learning approaches. https://doi.org/10.26182/5C5BA16237B57

Bery AA, Saad R. 2012. Tropical clayey sand soil's behaviour analysis and its empirical correlations via geophysics electrical resistivity method and engineering soil characterizations. International Journal of Geosciences.3:111–6.

Calamita G, Brocca L, Perrone A, Piscitelli S, Lapenna V, Melone F. Electrical resistivity and TDR methods for soil moisture estimation in central Italy test sites. Journal of Hydrology. 2012; 454–455:101–12.

Devi, A., Israil, M., Anbalagan, R., Gupta, P.K., 2017. Subsurface soil characterization using geoelectrical and geotechnical investigation at bridge site in Uttarakhand Himalayan region. J. Appl. Geophys. 144, 78–85.

De Vita, P., Di Maio, R., Piegari, E., 2012. A study of the correlation between electrical resistivity and matric suction for unsaturated ash-fall pyroclastic soils in the Campania Region (southern Italy). Environ. Earth Sci. 67 (3), 787–798. doi:10.1007/s12665-012-1531-4.

Fenton GA, Griffiths D. Bearing-capacity prediction of spatially random c φ soils. Canadian Geotechnical Journal. 2003; 40(1):54–65.

Gonçalves, J. T. D., Botelho, M. A. B., Machado, S. L., & Netto, L. G. (2021). Correlation between field electrical resistivity and geotechnical SPT blow counts at tropical soils in Brazil. Environmental Challenges, 5, 100220.

Loke, M., Barker, R., 1996. Rapid least-square inversion of apparent resistivity pseudo sections by a quasi-newton method. Geophys. Prospect. 44, 131–152. doi:10.1111/j.1365-2478. 1996.tb00142.x.

Liu S, Zha F, Yu X (2006). Laboratory Measurement Techniques of The Electrical Resistivity of Soils, J. of Eng. Geology, Vol.14(2): 216-222.

Osman S, Baharom S, Harith T, Zahir Z. 2010. Correlation of electrical resistivity with some soil properties in predicting factor of safety in slopes using simple multi meter. Conference on Sustainable Building and Infrastructure, Kuala Lumpur.

Ozcep F, Tezel O, Asci M (2009). Correlation between Electrical Resistivity and Soil-Water Content: Istanbul and Golcuk, Int. J. Phys. Sci. 4(6): 362-365

Pozdnyakov A, Pozdnyakova L, Karpachevskii L. Relationship between water tension and electrical resistivity in soils. Eurasian Soil Science. 2006; 39(1):S78–S83.

Samouëlian A, Cousin I, Tabbagh A, Bruand A, Richard G. Electrical resistivity survey in soil science: A review. Soil and Tillage Research. 2005; 83(2):173–93.

Sass, O., Bell, R., Glade, T., 2008. Comparison of GPR, 2-D resistivity and traditional techniques for the subsurface exploration of the O¨schingen landslide, swabian alb (Germany). Geomorphology 93, 89–103. doi:10.1016/j.geomorph.2006.12.019.

Goodfellow, I., Bengio, Y., & Courville, A. (2016). Deep learning. MIT Press.

Heaton, J. (2008). Introduction to Neural Networks for Java, 2nd Edition. Heaton Research, Inc.

Kingma, D. P., & Ba, J. (2015). Adam: A method for stochastic optimization. In Proceedings of the 3rd International Conference on Learning

Representations (ICLR). https://arxiv.org/abs/1412.6980

Prechelt, L. (1998). Early stopping—but when? In Neural Networks: Tricks of the Trade (pp. 55–69). Springer. https://doi.org/10.1007/3-540-49430-8_3

Rumelhart, D. E., Hinton, G. E., & Williams, R. J. (1986). Learning representations by back-propagating errors. Nature, 323(6088), 533–536. https://doi.org/10.1038/323533a0

Zhang, G. P., Patuwo, B. E., & Hu, M. Y. (1998). Forecasting with artificial neural networks: The state of the art. International Journal of Forecasting, 14(1), 35–62. https://doi.org/10.1016/S0169-2070(97)00044-7

Chai, T., & Draxler, R. R. (2014). Root mean square error (RMSE) or mean absolute error (MAE)? – Arguments against avoiding RMSE in the literature. Geoscientific Model Development, 7(3), 1247–1250. https://doi.org/10.5194/gmd-7-1247-2014

Draper, N. R., & Smith, H. (1998). Applied Regression Analysis (3rd ed.). Wiley.

Friedman, J., Hastie, T., & Tibshirani, R. (2001). The Elements of Statistical Learning: Data Mining, Inference, and Prediction. Springer.

Huber, P. J. (1964). Robust Estimation of a Location Parameter. Annals of Mathematical Statistics, 35(1), 73–101. https://doi.org/10.1214/aoms/1177703732

Hyndman, R. J., & Koehler, A. B. (2006). Another look at measures of forecast accuracy. International Journal of Forecasting, 22(4), 679–688. https://doi.org/10.1016/j.ijforecast.2006.03.001

Jiang, J., Wang, L., & Hu, X. (2020). Evaluating regression models for log-scale target variables: MSLE vs RMSE. Journal of Computational Science, 41, 101081. https://doi.org/10.1016/j.jocs.2020.101081

Kutner, M. H., Nachtsheim, C. J., & Neter, J. (2005). Applied Linear Regression Models (4th ed.). McGraw-Hill/Irwin.

Leys, C., Ley, C., Klein, O., Bernard, P., & Licata, L. (2013). Detecting outliers: Do not use standard deviation around the mean, use absolute deviation around the median. Journal of Experimental Social Psychology, 49(4), 764–766. https://doi.org/10.1016/j.jesp.2013.03.013

Makridakis, S. (1993). Accuracy measures: theoretical and practical concerns. International Journal of Forecasting, 9(4), 527–529.

Rodgers, J. L., & Nicewander, W. A. (1988). Thirteen Ways to Look at the Correlation Coefficient. The American Statistician, 42(1), 59–66. https://doi.org/10.2307/2685268

Willmott, C. J. (1982). Some Comments on the Evaluation of Model Performance. Bulletin of the American Meteorological Society, 63(11), 1309–1313. https://doi.org/10.1175/1520-0477(1982)063<1309:SCOTEO>2.0.CO;2

Willmott, C. J., & Matsuura, K. (2005). Advantages of the mean absolute error (MAE) over the root mean square error (RMSE) in assessing average model performance. Climate Research, 30, 79–82. https://doi.org/10.3354/cr030079

Zar, J. H. (2005). Spearman Rank Correlation. In Biostatistical Analysis (5th ed.). Pearson.

Goodfellow, I., Bengio, Y., & Courville, A. (2016). *Deep Learning*. MIT Press.

Strang, G. (2016). *Introduction to Linear Algebra* (5th ed.). Wellesley Cambridge Press.

Bishop, C. M. (2006). *Pattern Recognition and Machine Learning*. Springer.